International Journal of Ambient Energy

ISSN: (Print) (Online) Journal homepage: https://www.tandfonline.com/loi/taen20

Thermal optimisation through multilayer convective flow of CuO- MWCNT hybrid nanofluid in a composite porous annulus

Rajeev Anandika, V. Puneeth, S. Manjunatha & Ali J. Chamkha

To cite this article: Rajeev Anandika, V. Puneeth, S. Manjunatha & Ali J. Chamkha (2022) Thermal optimisation through multilayer convective flow of CuO- MWCNT hybrid nanofluid in a composite porous annulus, International Journal of Ambient Energy, 43:1, 6463-6473, DOI: 10.1080/01430750.2021.2023044

To link to this article: https://doi.org/10.1080/01430750.2021.2023044

Published online: 20 Jan 2022.

INTERNATIONAL JOURNAL OF AMBIENT ENERGY
2022, VOL. 43, NO. 1, 6463–6473
https://doi.org/10.1080/01430750.2021.2023044

Taylor & Francis
Taylor & Francis Group

Thermal optimisation through multilayer convective flow of CuO- MWCNT hybrid nanofluid in a composite porous annulus

Rajeev Anandika[a], V. Puneeth [a], S. Manjunatha[b] and Ali J. Chamkha[c]

[a]Department of Mathematics, CHRIST (Deemed to be University), Bengaluru, India; [b]Department of Sciences and Humanities, CHRIST (Deemed to be University), Bengaluru, India; [c]Faculty of Engineering, Kuwait College of Science and Technology, Doha District, Kuwait

ABSTRACT

The present article deals with the analysis of the three-layer convective flow of immiscible nanofluids in a composite porous annulus. Water and kerosene are chosen as base fluids due to their immiscible property that leads to the formation of a non-physical boundary separation and thus forming a multi-layer flow. In this model, the hybrid nanofluid is formed by suspending copper oxide (CuO) and multi walled carbon nanotubes (MWCNTs) in water which is sandwiched between layers of nanofluid formed by suspending CuO in kerosene leading to two boundary separations that give rise to the interface regions. Such a flow finds applications in the field of solar reactors, electronic cooling, etc. The model based on the above assumptions is in the form of a system of ordinary differential equations that are solved using the differential transformation method. The solutions are found to be in agreement with the existing literature and the results of this study are interpreted graphically. It is to be noted that the interfacial region in the multilayer nanofluid flow helps in maintaining the system at an optimum temperature which helps to cool down the systems. Further, the increase in the Eckert number increases the heat conduction of the nanofluid and pressure enhances the flow speed of the nanofluid.

ARTICLE HISTORY
Received 1 November 2021
Accepted 10 December 2021

KEYWORDS
Multi-layer flow; porous annulus; hybrid nanofluid; heat source/sink; differential transformation method

Nomenclature

μ	dynamic viscosity ($kgm^{-1}s^{-1}$)
ν	kinematic viscosity ($kgm^{-1}s^{-1}$)
ρ	density (kgm^{-3})
U_i,	velocity component for r directions (ms^{-1})
X, r	Cartesian coordinates(m)
g	gravitational acceleration (ms^{-2})
P	pressure ($kgm^{-1}s^{-2}$)
βt	coefficient of thermal expansion
T	temperature (K)
Cp	specific heat at constant pressure (m^2s^{-2})
C	nanoparticle concentration
Q	internal heat source
θ	dimensionless temperature
ϕ	dimensionless concentration
N	porosity parameter
β_c	coefficient of volumetric expansion
γ	chemical reaction parameter
κ	permeability of porous medium (m^2)
δ	dimensionless internal heat source
K_T	thermal diffusion ratio
Pr	Prandtl number
Gr_t	local temperature Grashof number
Gr_c	local mass Grashof number
λ_t	modified temperature Grashof number
λ_c	modified mass Grashof number
T_{w_1}, T_{w_2}	temperature at lower and upper wall (K)
k	thermal conductivity ($WK^{-1}m^{-1}$)
C_{w_1}, C_{w_2}	nanoparticle concentration at lower and upper wall
D	coefficient of mass diffusivity (m^2s^{-1})
Ec	Eckert number
Re	Reynolds number
Subscripts	
1	nanoliquid
i	Region *I*,*II* and *III*
f	base liquid
np	nanoparticle
2	hybrid nanoliquid

1. Introduction

The analysis of heat transfer finds lots of applications in many industries. The development of materials having high thermal conductivity and a faster transport rate of heat is essential in engineering and industrial processes. Thus, the studies on nanofluids have attracted many researchers across the world. These fluids are formed by suspending metallic particles of size 10^{-9} m. Since these particles have a higher thermal conductivity than the fluids, they aid in enhancing the thermal conductivity. These fluids find applications in industrial cooling, heaters/coolers, microelectronic equipment, automobiles, etc. For instance, nanofluids are used in vehicles to improve the efficiency of heat exchangers and cooling systems. In this regard, Farooq et al. (2016) analysed the non-linear radiation for the flow of viscoelastic nanofluid at the stagnation point. Hayat

CONTACT S. Manjunatha manjubhushana@gmail.com

et al. (2015) and Hayat, Shafiq, and Alsaedi (2014) performed a heat transfer analysis of third grade nanofluid under the influence of Lorentz force. Later, Shafiq et al. (2014) extended this study to analyse the unsteady flow of Williamson fluid. Whereas Choi et al. (2021) conducted an experiment to study the impact of nanoparticle migration in EG/water-based Al_2O_3 nanofluids. Shafiq, Çolak, and Sindhu (2021) and Naseem et al. (2018) had analysed the solid–fluid interface coating of CNT (carbon nanotubes) and its effect at the boundary interface. In the ethanol condensation process, the heat transfer properties of water-based nanofluids suspended with metals, metal oxides and carbon were studied by Banisharif et al. (2021) and Shafiq, Hammouch, and Sindhu (2017). Many studies have been conducted on various kinds of non newtonian nanofluids like Walter's B nanofluid (Shafiq et al. 2021), tangent hyperbolic nanofluid (Zari et al. 2021) and casson nanofluid (Shafiq et al. 2021) to reach the demands of industries in the process of heat transfer.

Though the nanofluids were capable of enhancing the thermal conductivity of traditional fluids, they lacked chemical stability. Hence in order to achieve stable nanofluid, researchers designed hybrid nanofluid in which two types of nanoparticles are suspended among which one of the nanoparticles enhances the thermal conductivity and the other ensures the inertness of the nanofluid. In this regard, Said et al. (2021) studied the generation of entropy and performed the analyses of linear Fresnel reflectors using hybrid nanofluids. Manjunatha et al. (2019) discussed the effect of variable viscosity for the flow of a hybrid nanofluid in the presence of natural convection. Ramesh et al. (2020) discussed the homogeneous–heterogeneous reactions for the flow of hybrid nanofluid composed of ND − Co_3O_4−EG. Abbas et al. (2021) studied the heat transfer in radiators made of aluminium tubes by allowing the Fe_3O_4 − TiO_2−water hybrid nanofluid. Fazeli, Emami, and Rashidi (2021) analysed the heat transfer performance of MWCNT − CuO hybrid nanofluid flowing in a fixed plate. These studies motivated Manjunatha et al. (2021) to frame a new mathematical model that describes the heat transfer of ternary hybrid nanofluids and observed that the heat conduction band to be higher for these nanofluids than the single-phase and two-phase nanofluids.

Recent studies show that the multilayer flow of nanofluids has gained more attention due to its higher heat transfer rate as well as its interfacial effects that help to understand the interactions between fluid layers. Especially, in analysing the flow of groundwater in coarse material that finds applications in hydrocarbon carbon spills and leaks. Multi-layer flow discusses the characteristics of fluid flow in two or more layers. Such a flow involving immiscible fluids has practical importance in the field of petroleum extraction, crude oil transport, chemical industries, geophysics, plasma physics, etc. Based on these applications, Vajravelu, Arunachalam, and Sreenadh (1995) studied the unsteady flow of fluids which was immiscible and observed the effect of magnetic field over velocity. Then Chamkha (2000) had given two immiscible fluid flow under porous and non-porous channels and mainly focused on heat absorption and the effect of buoyancy current. Malashetty, Umavathi, and Kumar (2004) focused on the two-layer flow of couple stress and viscous fluid and analysed the flow for strong, weak, and comparable porosity conditions with the couple stress fluid parameter. Kumar et al. (2010) discussed the effect of magnetic field on multilayer flow of micropolar fluid under a porous medium. Recently, Manjunatha et al. (2021) analysed the multilayer flow of a hybrid nanofluid in porous media. Rajeev and Mahanthesh (2021) discussed non-linear Boussinesq approximation in the multilayer flow of nanofluid.

The process of heat and mass transfer in porous medium has grabbed the attention of various researchers in recent years due to its wide applications in many engineering and thermal applications like packed-bed heat exchangers, catalytic reactors, thermal insulation, petroleum industries, electronic cooling, etc. Moreover, significant progress was observed in using the porous medium in biomedical applications such as drug delivery, tissue replacement, medical imaging, tissue culturing, etc. Due to these abundant applications, studies related to porous medium are in huge demand. For instance, Abo-Dahab et al. (2021) analysed the effect of suction and blowing over the flow of Casson nanofluid past a hot porous surface. Yadav, Chu, and Li (2021) examined the convection instability in the vertical flow of a nanofluid over a porous medium having considered variable gravity. Ying et al. (2021) conducted the thermo-hydraulic analysis with molten salt-based nanofluid and porous medium. El-Shorbagy et al. (2021) performed numerical analysis to study the effect of mixed convection in a porous trapezoidal channel and Al-Farhany and Abdulsahib (2021) studied mixed convection in two layers of the saturated porous medium. Ebrahimi et al. (2021) performed heat transfer analysis in the presence of mixed convection for nanofluid flowing in a closed elbow-shaped cavity. Valizadeh Ardalan et al. (2021) studied the unsteady flow of Cu − H_2O nanofluid in the presence of mixed convection.

An annulus is the space between two concentric objects of the same shape in which a larger one surrounds a smaller one. Due to their technological uses in compact heat exchangers, nuclear reactors, thermal storage systems, gas-insulated transmission lines, etc., heat transfer in the annulus in the presence of convection plays a significant role in engineering systems. Mixed convection exists when the currents of the natural convection possess the same order of magnitude as forced flow velocities and when forced and natural convection together contribute to the heat transfer, mixed convection occurs. The contribution of each of these convection mechanisms is dependent on the flow pattern and the magnitude of the temperature driving force. In this regard, Shahsavar et al. (2021) considered eccentric annulus to analyse the effect of free convection through the first and second law of thermodynamics. Shahsavar et al. (2021) have also given the details on entropy generation for the flow of Ag − H_2O nanofluid in a horizontal annulus. Miles and Bessaih (2021) performed the analysis of entropy generation for the fluids flowing past a cylindrical annulus. Mirzaie and Lakzian (2021) discussed the effect of natural convection near the density inversion point for the nanofluid flowing in a cylindrical annulus. Abd-Allah and Alsedais (2021) studied the impact of magnetic field on the heat and mass profile of nanofluid flowing in an annulus between a cavity and an elliptical obstacle.

Through the detailed literature survey performed, it is observed that no article exists that deals with the flow of CuO − MWCNT−water hybrid nanofluid in between the layers

of CuO−kerosene nanofluid in a concentric porous annulus. Hence, the authors make a sincere effort to analyse such a characteristic flow. The choice of two immiscible fluids, namely, water and kerosene as base fluids give rise to interfacial boundary regions. The selection of CuO as one of the nanoparticles makes this model useful in various technologies like catalysis, energy conversion, magnetic storage, energy storage, thermites, as well as superconductors and they help in achieving chemical stability. The CuO acts as a transition metal due to its high thermo-electrical capacity and nontoxic nature. It can be easily produced and is also available in affordable price; thus, engineers suggest this for better commercial applications. Furthermore, the middle region is suspended with an additional nanoparticle, namely *MWCNT* that ensures better heat capacity. Due to these applications and advantages, the authors have framed a mathematical model in the form of a system of differential equations that is solved by the differential transformation method and the results are interpreted through the tables and graphs.

2. Mathematical model

Figure 1 represents an infinitely long porous annulus made of two concentric cylinders with radii $\frac{R}{2}$ and $2R$ that contains a three-layered flow of immiscible nanofluids. The base fluids are assumed to be incompressible and the fluid flow is assumed to be steady and laminar. The region $R \leq r \leq \frac{3R}{2}$ contains porous medium and is filled with CuO-MWCNT hybrid nanofluid with water as the base fluid. The other two regions $\frac{R}{2} \leq r \leq R$ and $\frac{3R}{2} \leq r \leq 2R$ are filled with CuO-kerosene nanofluid. The pressure gradient is assumed to be common in all the regions. The temperature (T_{w_2}) and nanoparticle concentration (C_{w_2}) are kept constant in the cylinder having radius $\frac{R}{2}$. Whereas the cylinder with radius $2R$ is held at T_{w_1} and C_{w_1} such that $T_{w_1} \leq T_{w_2}$ and $C_{w_1} \leq C_{w_2}$. The Boussinesq approximation and viscous dissipation are taken into account and all the thermophysical properties of nanoparticles and the base fluid are assumed to be constant. The fully developed vertical flow of the nanofluids is assumed. The heat source, as well as chemical reaction, is considered in this model to obtain the realistic results. With these assumptions, the Mathematical model takes the following form (Abbas and Hasnain 2017):

Region I -CuO -kerosene nanofluid

$$\frac{\mu_1}{\rho_1}\left(\frac{d^2u_1}{dr^2}+\frac{1}{r}\frac{du_1}{dr}\right)-\frac{1}{\rho_1}\frac{\partial P}{\partial x} + \left(g\beta_{t_1}(T_1-T_{w_2})+g\beta_{c_1}(C_1-C_{w_2})\right)=0, \quad (1)$$

$$\alpha_1\left(\frac{d^2T_1}{dr^2}+\frac{1}{r}\frac{dT_1}{dr}\right)+\frac{\mu_1}{\rho_1 C_{p_1}}\left(\frac{du_1}{dy}\right)^2 + \frac{Q_1}{\rho_1 C_{p_1}}\left(T_1-T_{w_1}\right)=0, \quad (2)$$

$$D_1\left(\frac{d^2C_1}{dr^2}+\frac{1}{r}\frac{dC_1}{dr}\right)-\gamma_1\left(C_1-C_{w_2}\right)=0. \quad (3)$$

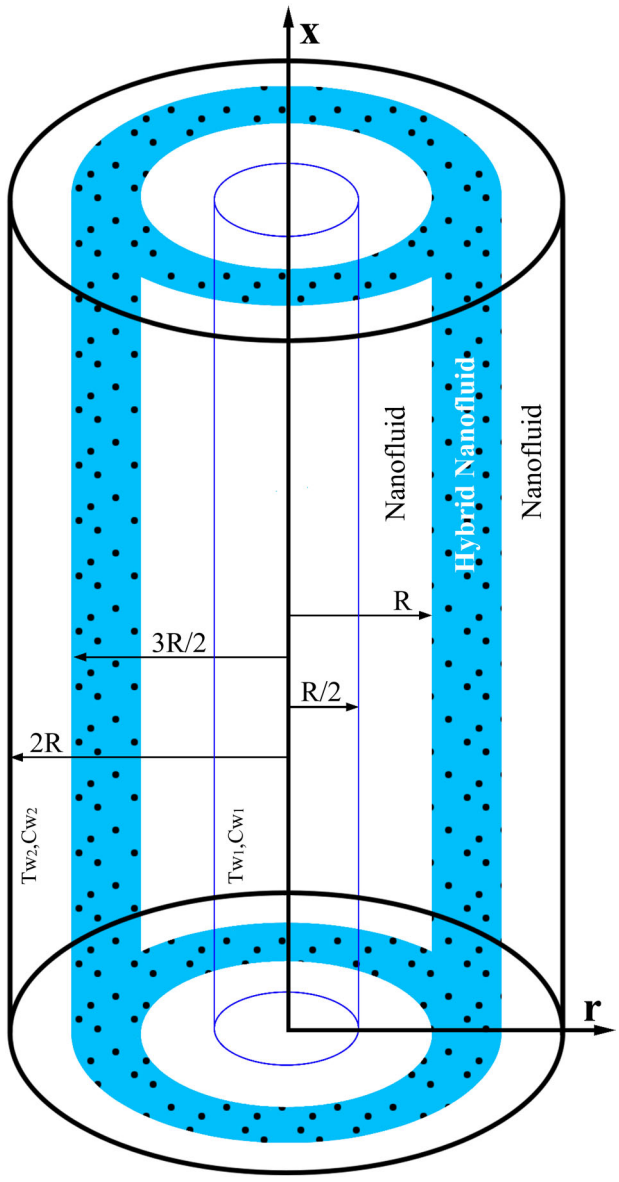

Figure 1. Geometry of the problem.

Region II -CuO- MWCNT -water Hybrid nanofluid

$$\frac{\mu_1}{\rho_2}\left(\frac{d^2u_2}{dr^2}+\frac{1}{r}\frac{du_2}{dr}\right)-\frac{1}{\rho_2}\frac{\partial P}{\partial x}-\frac{\psi\mu_2}{\rho_2\kappa}u_2 + \left(g\beta_{t_2}(T_2-T_{w_2})+g\beta_{c_2}(C_2-C_{w_2})\right)=0, \quad (4)$$

$$\alpha_2\left(\frac{d^2T_2}{dr^2}+\frac{1}{r}\frac{dT_2}{dr}\right)+\frac{\mu_2}{\rho_2 C_{p_2}}\left(\frac{du_2}{dy}\right)^2 + \frac{Q_2}{\rho_2 C_{p_2}}\left(T_2-T_{w_2}\right)+\frac{\psi\mu_2}{\rho_2 C_{p_2}\kappa}u_2^2=0, \quad (5)$$

$$D_2\left(\frac{d^2C_2}{dr^2}+\frac{1}{r}\frac{dC_2}{dr}\right)-\gamma_2\left(C_2-C_{w_2}\right)=0. \quad (6)$$

Region III -CuO-kerosene Nanofluid

$$\frac{\mu_1}{\rho_1}\left(\frac{d^2u_3}{dr^2}+\frac{1}{r}\frac{du_3}{dr}\right)-\frac{1}{\rho_1}\frac{\partial P}{\partial x}$$

$$+\left(g\beta_{t_1}(T_3-T_{w_2})+g\beta_{c_1}(C_3-C_{w_2})\right)=0, \tag{7}$$

$$\alpha_1\left(\frac{d^2T_3}{dr^2}+\frac{1}{r}\frac{dT_3}{dr}\right)+\frac{\mu_1}{\rho_1 C_{p_1}}\left(\frac{du_3}{dy}\right)^2+\frac{Q_1}{\rho_1 C_{p_1}}\left(T_3-T_{w_1}\right)=0, \tag{8}$$

$$D_1\left(\frac{d^2C_3}{dr^2}+\frac{1}{r}\frac{dC_3}{dr}\right)-\gamma_1\left(C_3-C_{w_2}\right)=0, \tag{9}$$

The boundary and interface conditions can be expressed as follows:

$$\begin{aligned}
&u_1(r)=0,\quad T_1(r)=T_{w_2},\\
&C_1(r)=C_{w_2},\ at\ r=\frac{R}{2}.\\
&u_2(r)=u_1(r),\quad T_2(r)=T_1(r),\\
&C_2(r)=C_1(r),\\
&\mu_1\frac{du_1}{dr}=\mu_2\frac{du_2}{dr},\quad k_1\frac{dT_1}{dr}=k_2\frac{dT_2}{dr},\\
&D_1\frac{dC_1}{dr}=D_2\frac{dC_2}{dr}\ \text{at}\ r=R.\\
&u_2(r)=u_3(r),\quad T_2(r)=T_3(r),\\
&C_3(r)=C_2(r),\\
&\mu_2\frac{du_2}{dr}=\mu_1\frac{du_3}{dr},\quad k_1\frac{dT_3}{dr}=k_2\frac{dT_2}{dr},\\
&D_1\frac{dC_3}{dr}=D_2\frac{dC_2}{dr}\text{at}\ r=\frac{3R}{2}.\\
&u_3(r)=0,\quad T_3(r)=T_{w_1},\\
&C_3(r)=C_{w_1},\ \text{at}\ r=2R.
\end{aligned} \tag{10}$$

where no slip condition for velocities is assumed, temperature and concentration are constant at $r=\frac{R}{2}$ and $r=2R$. At the interface, the velocities and stress, temperature and heat flux, concentration and mass flux are equal. In order to simplify the governing equations, Equations (1)–(9) have to be nondimensionalised with the help of the following non-dimensional quantities:

$$\begin{aligned}
&u_i^*=\frac{u_i}{u_0},\quad r^*=\frac{r}{R},\ \theta_i=\frac{T_i-T_{w_2}}{T_{w_1}-T_{w_2}},\\
&\phi_i=\frac{C_i-C_{w_2}}{C_{w_1}-C_{w_2}},\\
&p_i=-\frac{R^2}{\mu_i u_0}\left(\frac{\partial P_i}{\partial x}\right),\quad Re_i=\frac{\rho_i R u_0}{\mu_i},\\
&Gt_i=\frac{g\rho_i^2\beta_{t_i(Tw_1-Tw_2)}R^3}{\mu_i^2},\\
&Gc_i=\frac{g\rho_i^2\beta_{ci}\,(Cw_1-Cw_2)\,R^3}{\mu_i^2}.
\end{aligned}$$

Using the thermophysical properties of *CuO* nanofluid and CuO-MWCNT hybrid nanofluid (Nallusamy, Narayanan, and Logeshwaran 2017; Nallusamy 2016) given in Table 1 along with the non-dimensional quantities, the above equations take the following form:

Region I: CuO -kerosene Nanofluid

$$A_1\left(\frac{d^2u_1}{dr^2}+\frac{1}{r}\frac{du_1}{dr}\right)+p_1+A_5\lambda_{t_1}\theta_1+A_{11}\lambda_{c_1}\phi_1=0, \tag{11}$$

$$A_9\left(\frac{d^2\theta_1}{dr^2}+\frac{1}{r}\frac{d\theta_1}{dr}\right)+A_1Pr_1Ec_1\left(\frac{du_1}{dy}\right)^2+Pr_1\delta_1\theta_1=0, \tag{12}$$

$$\left(\frac{d^2\phi_1}{dr^2}+\frac{1}{r}\frac{d\phi_1}{dr}\right)-\chi_1\phi_1=0, \tag{13}$$

Region II: CuO- MWCNT -water hybrid nanofluid

$$A_2\left(\frac{d^2u_2}{dr^2}+\frac{1}{r}\frac{du_2}{dr}\right)+p_2-A_2Nu_2+A_6\lambda_{t_2}\theta_2+A_{12}\lambda_{c_2}\phi_2=0, \tag{14}$$

$$A_{10}\left(\frac{d^2\theta_2}{dr^2}+\frac{1}{r}\frac{d\theta_2}{dr}\right)+A_2Pr_2Ec_2\left(\left(\frac{du_2}{dy}\right)^2+Nu_2^2\right)+Pr_2\delta_2\theta_2=0, \tag{15}$$

$$\left(\frac{d^2\phi_2}{dr^2}+\frac{1}{r}\frac{d\phi_2}{dr}\right)-\chi_2\phi_2=0, \tag{16}$$

Region III: CuO -kerosene nanofluid

$$A_1\frac{d^2u_3}{dy^2}+p_1+A_5\lambda_{t_1}\theta_3+A_{11}\lambda_{c_1}\phi_3=0, \tag{17}$$

$$A_9\left(\frac{d^2\theta_3}{dr^2}+\frac{1}{r}\frac{d\theta_3}{dr}\right)+A_1Pr_1Ec_1\left(\frac{du_3}{dy}\right)^2+Pr_1\delta_1\theta_3=0, \tag{18}$$

$$\left(\frac{d^2\phi_3}{dr^2}+\frac{1}{r}\frac{d\phi_3}{dr}\right)-\chi_1\phi_3=0, \tag{19}$$

The dimensionless boundary and interface conditions take the following form:

$$\begin{aligned}
&u_1=0,\quad \theta_1=0,\ \phi_1=0,\ at\ r=0.5.\\
&u_2=u_1,\quad \theta_2=\theta_1,\ \phi_2=\phi_1,\\
&\frac{du_1}{dr}=\mu\frac{du_2}{dr},\quad \frac{d\theta_1}{dr}=k\frac{d\theta_2}{dr},\ \frac{d\phi_1}{dr}=D\frac{d\phi_2}{dr}\text{at}\ r=1.\\
&u_2=u_3,\quad \theta_2=\theta_3,\ \phi_2=\phi_1,\\
&\mu\frac{du_2}{dr}=\frac{du_3}{dr},\quad k\frac{d\theta_2}{dr}=\frac{d\theta_3}{dr},\ D\frac{d\phi_2}{dr}=\frac{d\phi_3}{dr}\text{at}\ r=1.5.\\
&u_3=0,\quad \theta_3=1,\ \phi_3=1\text{at}\ r=2.
\end{aligned} \tag{20}$$

Furthermore, to measure the difference of three-layer nanofluids, the ratios of the physical properties are defined as follows:

$$\begin{aligned}
&\lambda_{t_i}=\frac{G_{t_i}}{Re},\quad \lambda_{c_i}=\frac{G_{c_i}}{Re},\ Pr_i=\frac{\mu_i C_{p_i}}{k_i},\\
&Ec_i=\frac{u_0^2}{C_{p_i}(T_{w_2}-T_{w_1})},\\
&\delta_i=\frac{Q_i R^2}{\mu_i C_{p_i}},\quad N=\frac{\psi R^2}{\kappa},\ \chi_i=\frac{\gamma_i R^2}{D_i},\ \mu=\frac{\mu_2}{\mu_1},
\end{aligned}$$

Table 1. Properties of CuO - kerosene nanofluid and CuO- MWCNT - water hybrid nanofluid.

Properties	-CuO − kerosene nanofluid	CuO − MWCNT − water hybrid nanofluid
Viscosity (Nm^{-2})	$\frac{\mu_{nf}}{\mu_f} = \frac{1}{(1-\Phi_{np_1})^{2.5}}$	$\frac{\mu_{hnf}}{\mu_f} = [1-(\Phi_{np_1}+\Phi_{np_2})]^{-2.5} (Where \quad \Phi = \Phi_{np_1}+\Phi_{np_2})$
Density (kgm^{-3})	$\frac{\rho_{nf}}{\rho_f} = \left[(1-\Phi_{np_1}) + \Phi_{np_1}\frac{\rho_{np_1}}{\rho_f}\right]$	$\frac{\rho_{hnf}}{\rho_f} = \left[(1-\Phi) + \Phi_{np_1}\frac{\rho_{np_1}}{\rho_f} + \Phi_{np_2}\frac{\rho_{np_2}}{\rho_f}\right]$
Heat capacity ($Jkg^{-1}K^{-1}$)	$\frac{(\rho Cp)_{nf}}{(\rho Cp)_f} = \left[(1-\Phi_{np_1}) + \Phi_{np_1}\frac{(\rho Cp)_{np_1}}{(\rho Cp)_f}\right]$	$\frac{(\rho Cp)_{hnf}}{(\rho Cp)_f} = \left[(1-\Phi) + \Phi_{np_1}\frac{(\rho Cp)_{np_1}}{(\rho Cp)_f} + \Phi_{np_2}\frac{(\rho Cp)_{np_2}}{(\rho Cp)_f}\right]$
Thermal conductivity ($Wm^{-1}K^{-1}$)	$\frac{k_{nf}}{k_f} = \frac{(k_{np_1}+2k_f)-2\Phi_{np_1}(k_f-k_{np_1})}{(k_{np_1}+2k_f)+2\Phi_{np_1}(k_f-k_{np_1})}$	$\frac{k_{hnf}}{k_f} = \left[\frac{(\frac{\Phi_{np_2}k_{np_2}+\Phi_{np_1}k_{np_1}}{\Phi}) + 2k_f + 2[\Phi_{np_2}k_{np_2}+\Phi_{np_1}k_{np_1}] - 2\Phi k_f}{(\frac{\Phi_{np_2}k_{np_2}+\Phi_{np_1}k_{np_1}}{\Phi}) + 2k_f - [\Phi_{np_2}k_{np_2}+\Phi_{np_1}k_{np_1}] + \Phi k_f}\right]$
Thermal expansion co-efficient (K^{-1})	$\frac{(\rho\beta_{ti})_{nf}}{(\rho\beta_{ti})_f} = \left[(1-\Phi_{np_1}) + \Phi_{np_1}\frac{(\rho\beta_{ti})_{np_1}}{(\rho_1\beta_1)_f}\right]$	$\frac{(\rho\beta_{ti})_{hnf}}{(\rho\beta_{ti})_f} = \left[(1-\Phi) + \Phi_{np_1}\frac{(\rho\beta_{ti})_{np_1}}{(\rho_2\beta_{ti})_f} + \Phi_{np_2}\frac{(\rho\beta_{ti})_{np_2}}{(\rho_2\beta_{ti})_f}\right]$
Volumetric expansion co-efficient (m^3)	$\frac{(\rho\beta_{ci})_{nf}}{(\rho\beta_{ci})_f} = \left[(1-\Phi_{np_1}) + \Phi_{np_1}\frac{(\rho\beta_{ci})_{np_1}}{(\rho_1\beta_1)_f}\right]$	$\frac{(\rho\beta_{ci})_{hnf}}{(\rho\beta_{ci})_f} = \left[(1-\Phi) + \Phi_{np_1}\frac{(\rho\beta_{ci})_{np_1}}{(\rho_2\beta_{ci})_f} + \Phi_{np_2}\frac{(\rho\beta_{ci})_{np_2}}{(\rho_2\beta_{ci})_f}\right]$

$$k = \frac{k_2}{k_1}, \quad D = \frac{D_2}{D_1}, p_2 = \frac{1}{\mu}p_1, Pr_2 = \frac{Cp\mu}{k}Pr_1,$$
$$Ec_2 = \frac{Ec_1}{Cp}, \quad \frac{\lambda_{t_2}}{\lambda_{t_1}} = \frac{\nu_1\beta_{t_2}}{\nu_1\beta_{t_2}}h^2, \frac{\lambda_{c_2}}{\lambda_{c_1}} = \frac{\nu_1\beta_{c_2}}{\nu_1\beta_{c_2}}h^2.$$

3. Solution procedure

The ordinary differential equations (11)–(19) are numerically solved using DTM (Odibat 2008). This method was derived from the Taylor series expansion and the transformation is given by

$$F(hl) = \frac{1}{h!}\left[\frac{d^h f(r)}{dr^h}\right]_{r=0} \tag{21}$$

and the inverse differential transformation is

$$f(r) = \sum_{h=0}^{\infty} F(h)r^h, \tag{22}$$

merging Equations (21) and (22) we get

$$f(r) = \sum_{h=0}^{\infty} \frac{r^h}{h!}\frac{d^h f(r)}{dy^h r}\bigg|_{y=0}. \tag{23}$$

Since $\sum_{h=0}^{\infty} F(h)r^h$ is trivial and can be ignored, so $u(r)$ can be formed as finite series and the equation can be noted as (Chen and Liu 2014)

$$f(r) = \sum_{h=0}^{n} F(h)r^h. \tag{24}$$

Where the value of n depends on the convergence requirements in real applications and differential transform of $f(r)$ is $F(r)$. On transforming Equations (11)–(19) we get.

Region I: CuO -kerosene nanofluid

$$\begin{aligned} &A_1(h+1)(h+2)U_1[h+2] \\ &\quad + \Delta(h-m)(h+1)U_1[h+1] - p_1\Delta(h-m) \\ &\quad + A_5\lambda_{t_1}\Theta_1[h] + A_{11}\lambda_{c_1}\Phi_1[h] = 0, \end{aligned} \tag{25}$$

$$\begin{aligned} &A_9(h+1)(h+2)\Theta_1[h+2] \\ &\quad + \Delta(h-m)(h+1)\Theta_1[h+1] + Pr_1\delta_1\Theta_1[h] \\ &\quad + A_1Ec_1Pr_1\sum_{h=0}^{h}(m+1)(h-m+1) \\ &\quad \times U_1[h-m+1]U_1[m+1] = 0, \end{aligned} \tag{26}$$

$$\begin{aligned} &(h+1)(h+2)\Phi_1[h+2] \\ &\quad + \Delta(h-m)(h+1)\Phi_1[h+1] + \chi_1\Phi_1[h] = 0, \end{aligned} \tag{27}$$

Region II: CuO- MWCNT-water hybrid nanofluid

$$\begin{aligned} &A_2(h+1)(h+2)U_2[h+2] \\ &\quad + \Delta(h-m)(h+1)U_2[h+1] - p_2\Delta(h-m) \\ &\quad - A_2NU_2[h] + A_6\lambda_{t_2}\Theta_2[h] + A_{12}\lambda_{c_2}\Phi_2[h] = 0, \end{aligned} \tag{28}$$

$$\begin{aligned} &A_{10}(h+1)(h+2)\Theta_2[h+2] \\ &\quad + \Delta(h-m)(h+1)\Theta_2[h+1] \\ &\quad + Pr_2\delta_2\Theta_2[h] + A_2Ec_2Pr_2 \\ &\quad \sum_{h=0}^{r}(m+1)(h-m+1)U_2[h-m+1]U_2[m+1] \\ &\quad + A_2Pr_2Ec_2N\sum_{h=0}^{h}(h-m)(h-m+1)U_2[m] = 0, \end{aligned} \tag{29}$$

$$\begin{aligned} &(h+1)(h+2)\Phi_2[h+2]+ \\ &\quad + \Delta(h-m)(h+1)\Phi_2[h+1] + \chi_2\Phi_2[h] = 0, \end{aligned} \tag{30}$$

Region III: CuO -kerosene nanofluid

$$\begin{aligned} &A_1(h+1)(h+2)U_3[h+2] \\ &\quad + \Delta(h-m)(h+1)U_3[h+1] - p_1\Delta(h-m) \end{aligned}$$

$$+ A_5\lambda_{t_1}\Theta_3[h] + A_{11}\lambda_{c_1}\Phi_3[h] = 0, \tag{31}$$

$$\begin{aligned} &A_9(h+1)(h+2)\Theta_1[h+2] \\ &\quad + \Delta(h-m)(h+1)\Theta_3[h+1] \\ &\quad + Pr_1\delta_1\Theta_3[h] \\ &\quad + A_1Ec_1Pr_1\sum_{l=0}^{h}(m+1)(h-m+1) \\ &\quad \times U_3[h-m+1]U_1[m+1] = 0, \end{aligned} \tag{32}$$

$$\begin{aligned} &(h+1)(h+2)\Phi_3[h+2] + \Delta(h-m)(h+1) \\ &\quad \times \Phi_3[h+1] + \chi_1\Phi_3[h] = 0, \end{aligned} \tag{33}$$

with the help of transformed boundary conditions, the problem is converted to an initial value problem and by using the recursive method, values for U_i, Θ_i and Φ_i can be calculated. Hence, the final solution can be obtained by substituting U_i, Θ_i and Φ_i in Equation (24).

4. Heat transfer rate and skin friction coefficient

Nusselt number: The rate of heat transfer depends on the temperature distribution on the channel wall to liquid which is given as follows:

$$q_B = \left(\frac{d\theta_1}{dr}.\right)_{r=0.5}, \quad q_T = \left(\frac{d\theta_3}{dr}\right)_{r=2}.$$

Skin friction: The skin friction at channel walls is given by

$$\tau_B = \left(\frac{du_1}{dr}\right)_{r=0.5}, \quad \tau_T = \left(\frac{du_3}{dr}\right)_{r=2}.$$

Sherwood number: The mass transfer rate for channel walls are given by

$$Sh_B = \left(\frac{d\phi_1}{dr}\right)_{r=0.5}, \quad Sh_T = \left(\frac{d\phi_3}{dr}\right)_{y=2}.$$

5. Results and discussions

The multilayer flow comprising of a layer of hybrid nanofluid in the middle of two nanofluid layers has been analysed. The hybrid nanofluid in the middle region is formed by adding MWCNT and CuO to water, whereas the other two layers of nanofluid are formed by suspending CuO into kerosene. The system of differential equations that govern such a flow is non-dimensionalised and solved using DTM. The obtained results coincide with the results achieved by Umavathi, Chamkha, and Shekar (2014) which is shown in Table 2. The outcomes of the study are rendered in this section through Figures 2–13.

The impact of thermal and mass Grashof number and pressure on velocity is depicted in Figures 2– 4 respectively. It is observed that these three parameters have a similar effect on the velocity profile. The increase in the thermal Grashof number indicates that the fluid is being heated and hence the density decreases as a result the velocity of the nanofluid increases for higher values of thermal Grashof number in all three regions as seen in Figure 2. Further, it can also be observed that the velocity of the fluid is maximum in the middle region than the two adjacent regions because of the low density of nanofluid upon conduction of heat. Similarly, the effect of mass Grashof number is shown in Figure 3. Due to various densities that create high viscosity and pressure loss, the pressure gradient for nanofluids and hybrid nanofluids formed with distinct base fluids is strong and thus the velocity increases as shown in Figure 4.

Table 2. Comparison table.

	Velocity (ms^{-1})		Temperature (K)	
y	Umavathi	Present	Umavathi	Present
−1	0	0	0	0
−0.5	1.25	1.25	0.1667	0.1667
0	2	2	0.3333	0.3333
0	2	2	0.3333	0.3333
0.5	2.25	2.25	0.5	0.5
1	2	2	0.6667	0.6667
1	2	2	0.6667	0.6667
1.5	1.25	1.25	0.8333	0.8333
2	0	0	1	1

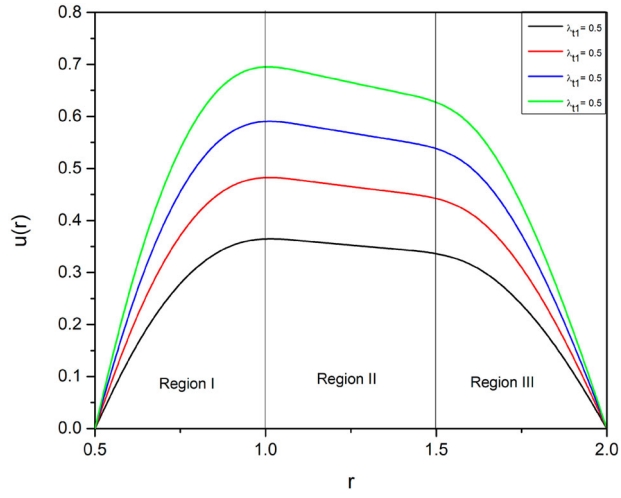

Figure 2. Outcome of the modified thermal Grashof number λ_t on velocity.

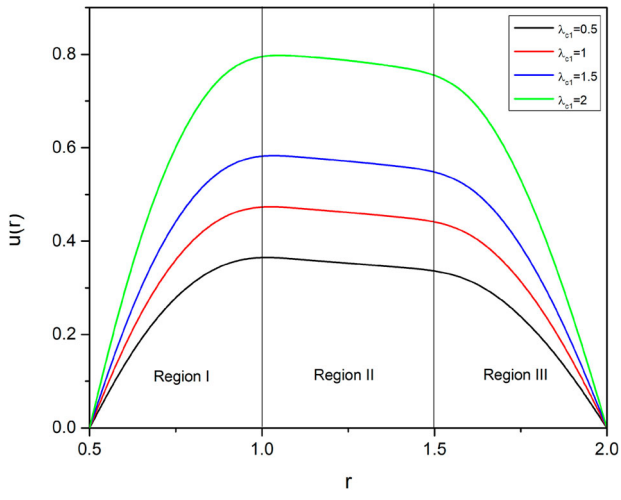

Figure 3. Outcome of modified mass Grashof number λ_c on velocity.

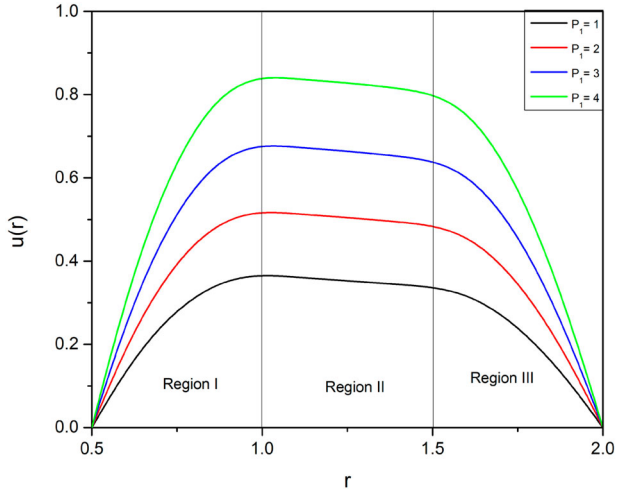

Figure 4. Outcome of pressure on velocity.

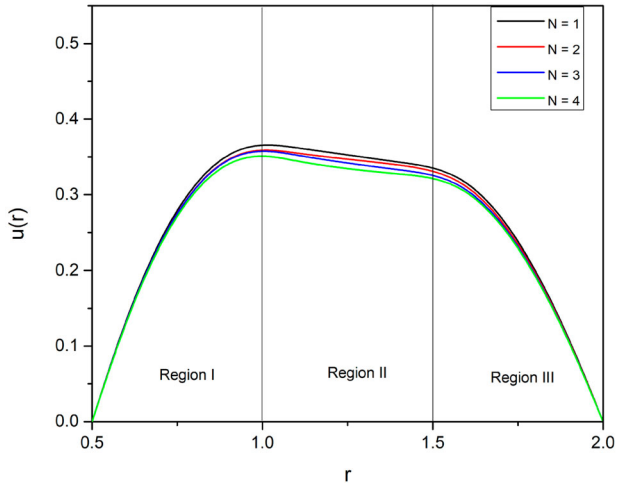

Figure 5. Outcome of porosity on velocity.

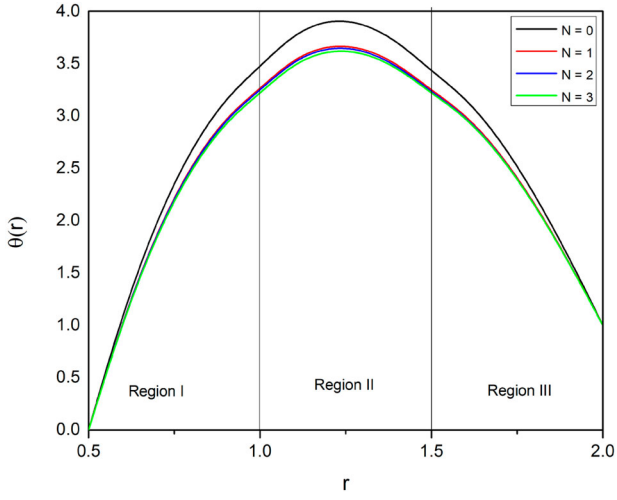

Figure 6. Outcome of porosity on temperature.

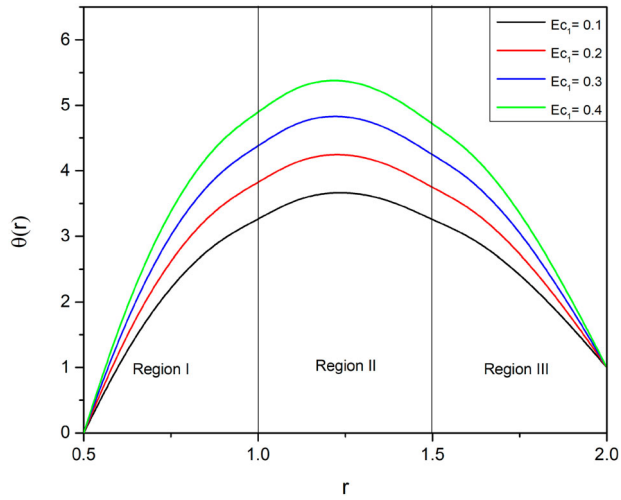

Figure 7. Outcome of *Ec* on temperature.

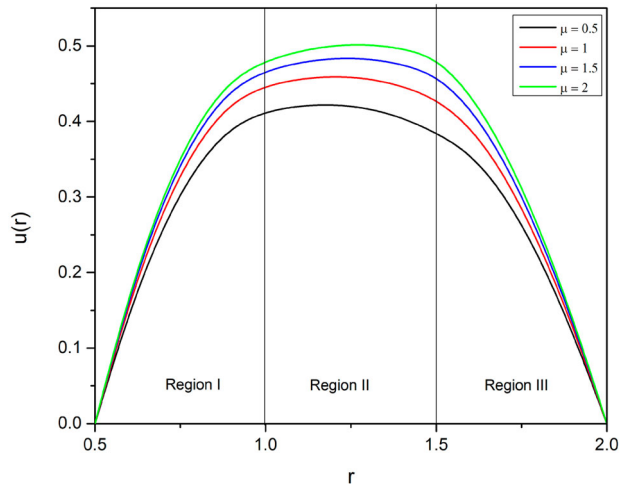

Figure 8. Outcome of ratios of viscosity on velocity.

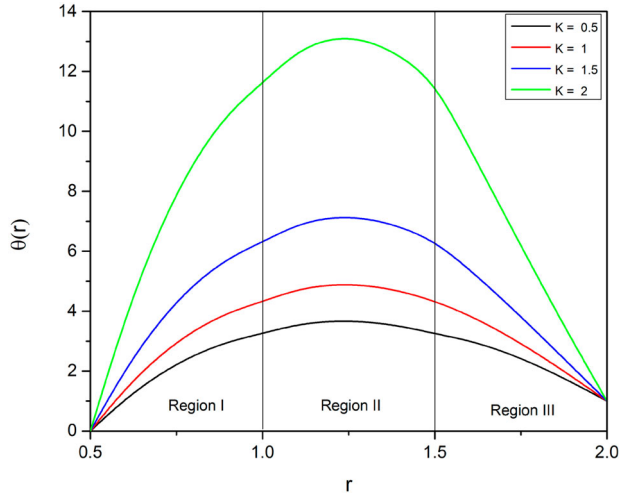

Figure 9. Outcome of ratios of thermal conductivity on temperature.

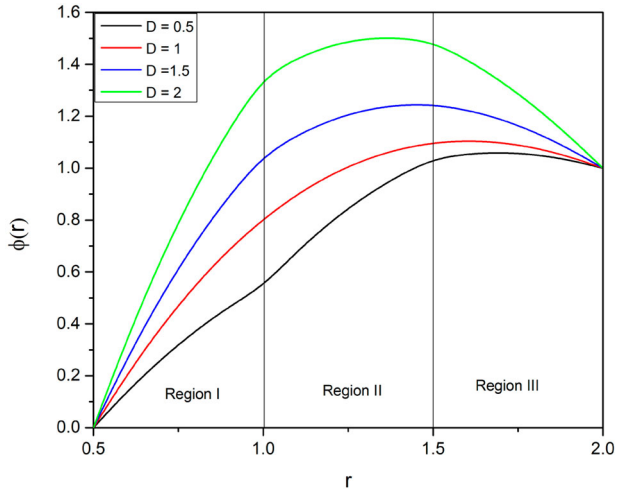

Figure 10. Outcome of ratios of mass diffusivity on concentration.

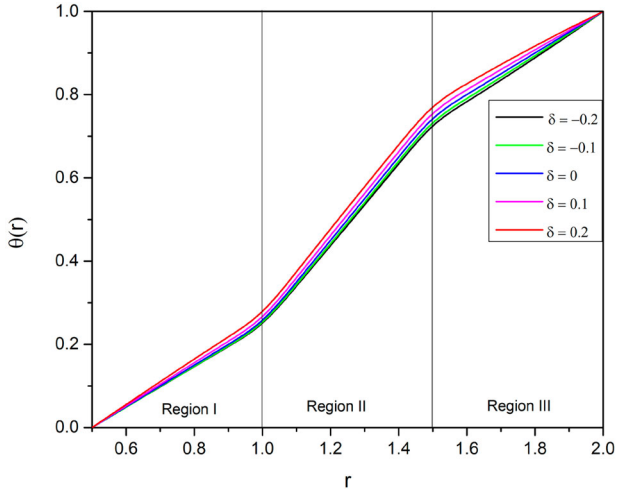

Figure 11. Outcome of heat source on temperature.

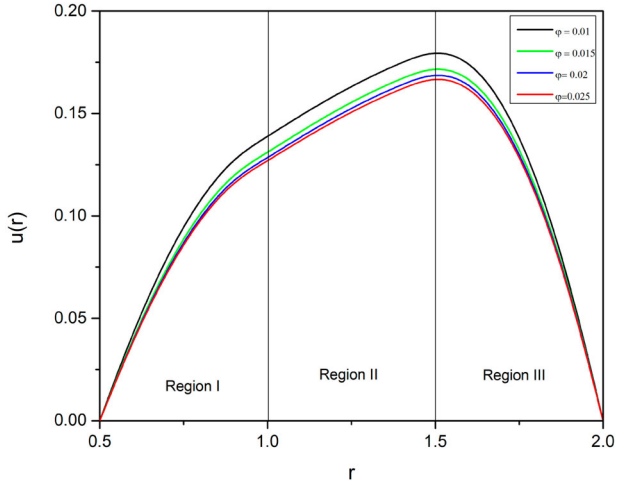

Figure 12. Outcome of nanoparticle volume fraction on velocity.

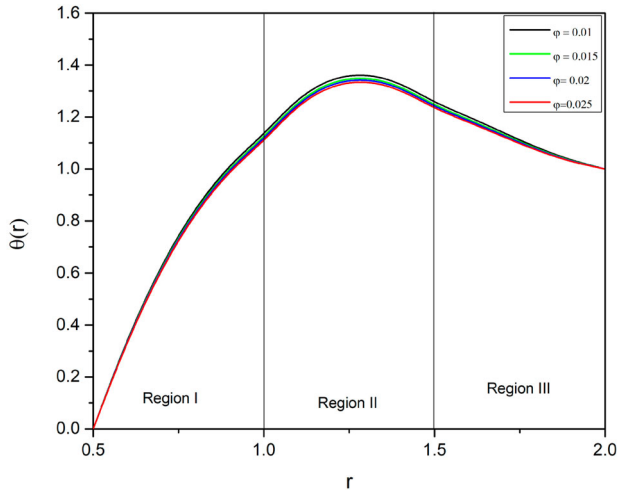

Figure 13. Outcome of nanoparticle volume fraction on temperature.

The viscosity of the nanofluid increases as a result of higher porosity, this will gradually cause the fluid to flow at a lower velocity as shown in Figure 5. It also shows that the effect of porous medium affects the flow near the interface region on either side but it has no impact far from the middle region. This is because the porous medium is considered only in the middle region. Meanwhile, the temperature of the nanofluid decreases with the increase in porosity parameter. The increase in the pores reduces the flow speed and their heat gets transferred from the nanofluid to the surface and results in the decreased temperature of the nanofluid as shown in Figure 6. The Eckert number is also known as the viscous dissipation parameter used to characterise the impact of self-heating of fluid due to internal friction. As a result, the temperature of the nanofluid increases with the increase in Eckert number as shown in Figure 7.

The effect of ratios of viscosity, thermal conductivity and mass diffusivity on the velocity, temperature and concentration profile is shown in Figures 8– 10. For a fixed viscosity in the middle region, the increase in the ratio of viscosity reduces the viscous force in the first and third regions which increase the velocity in these two regions. As a result, the layers at the interfacial regions pull the hybrid nanofluid in the middle region and hence an increase in the velocity of the nanofluid is observed in Figure 8. Whereas the fluid flow remains constant in the middle region due to the fact that its viscosity is left unaltered. Meanwhile, the increase in the thermal conductivity ratio enhances the conduction band in regions I and III. The interface regions will assist in developing the thermal conductance of the heat in the middle region as well hence an increase in the heat transfer is seen in Figure 9 for higher values of thermal conductance ratios. Similarly, the effect of mass diffusivity is seen in Figure 10.

The presence of a heat source is considered for positive values of Q and this source will constantly generate heat so that the temperature of the nanofluid increases. The presence of a heat sink is considered when the values of Q are chosen to be negative. This sink will absorb heat from the nanofluid as a result, the temperature of the nanofluid decreases for negative values of Q. This effect is depicted in Figure 11 which also shows that the heat conduction in the middle layer is much greater than the

Table 3. Values for skin friction coefficients, Nusselt number and Sherwood number.

		q_B	q_T	τ_B	τ_T	Sh_B	Sh_T
G_{t_1}	0.5	1.9509	−4.3257	5.3745	−28.3166	0.3461	−2.2068
	1	2.0927	−6.8562	5.9004	−33.4486	0.3461	−2.2068
	1.5	2.1765	−9.3721	6.2162	−37.3408	0.3461	−2.2068
	2	2.2904	−11.788	6.3656	−39.572	0.3461	−2.2068
G_{c_1}	0.5	1.9509	−4.3257	5.3745	−28.3166	0.3461	−2.2068
	1	2.4525	−5.6561	6.1935	−32.3056	0.3461	−2.2068
	1.5	3.2538	−8.8976	8.1014	−43.6865	0.4249	−6.3923
	2	3.8052	−10.9968	9.7729	−53.6844	0.4249	−6.3923
Ec_1	0.1	1.9509	−4.3257	5.3745	−28.3166	0.3461	−2.2068
	0.2	1.8104	−4.7069	6.5407	−35.3677	0.3461	−2.2068
	0.3	1.6873	−5.0316	7.578	−42.7641	0.3461	−2.2068
	0.4	1.5831	−5.2876	8.478	−49.9606	0.3461	−2.2068
N	1	1.8843	−4.1571	5.3507	−28.686	0.3461	−2.2068
	2	1.9521	−4.2031	5.31	−27.9638	0.3461	−2.2068
	3	1.9593	−4.2074	5.3572	−27.8347	0.3461	−2.2068
	4	1.9668	−4.212	5.3388	−27.7869	0.3461	−2.2068
P_1	0.5	1.9509	−4.3257	5.3745	−28.3166	0.3461	−2.2068
	1	2.8809	−5.8063	6.7402	−33.2446	0.3461	−2.2068
	1.5	2.9267	−7.505	8.6186	−40.4236	0.3461	−2.2068
	2	4.6333	−9.4135	11.0073	−50.512	0.3461	−2.2068
δ_1	−2	1.2333	−1.2308	0.0758	−4.8663	0.3461	−2.2068
	−1	1.373	−1.3897	1.0607	−10.9456	0.3461	−2.2068
	1	1.7468	−3.1295	4.0094	−26.4361	0.3461	−2.2068
	2	1.9509	−4.3257	5.3745	−28.3166	0.3461	−2.2068
μ	0.5	1.8845	−4.2798	5.3937	−29.1158	0.3461	−2.2068
	1	1.9596	−4.2268	6.4791	−29.5978	0.3461	−2.2068
	1.5	1.9891	−4.1931	6.9875	−30.0408	0.3461	−2.2068
	2	2.0044	−4.1696	7.2913	−30.4016	0.3461	−2.2068
k	0.5	1.8845	−4.2798	5.3937	−29.1158	0.3461	−2.2068
	1	2.0273	−4.1978	6.9943	−26.4292	0.3461	−2.2068
	1.5	2.3189	−4.05	10.0805	−21.1304	0.3461	−2.2068
	2	3.0749	−3.7333	18.3424	−5.7933	0.3461	−2.2068
D	0.5	1.9596	−4.2268	5.4791	−29.5978	0.3461	−2.2068
	1	2.1318	−4.3249	5.6131	−29.6231	0.5098	−2.1961
	1.5	2.3553	−4.4461	5.8483	−29.9178	0.6639	−2.1711
	2	2.6236	−4.6482	6.1697	−30.6691	0.8555	−2.1303

other two layers. This occurs because of the fact that the middle layer is considered to be a hybrid nanofluid. The impact of volume fraction over the velocity and thermal profile is shown in Figures 12 and 13, respectively. The increase in the volume fraction contributes to the increased density that would further decrease the velocity of the fluid flow as shown in Figure 12. Furthermore, the temperature of the nanofluid decreases with the increase in the volume fraction of *MWCNT* due to the interfacial effect that arises at the boundary formed due to the immiscible fluids.

The variations of the skin friction coefficient, Nusselt number and Sherwood number for changes in various fluid flow parameters are depicted in Table 3. The Sherwood number shows deflection only for the changes in Gc_1 and D. For all other parameters, it remains constant. The increase in mass Grashof number enhanced the Sherwood number at radius $r = 0.5$ and an opposite trend is seen in the wall at $r = 2$. Whereas the increase in D enhances the rate of heat transfer at $r = 0.5$ and decreases the heat transfer rate at $r = 2$. It has a similar impact on the skin friction coefficients also. Meanwhile, the rise in the values of Gc_1 increases the skin friction coefficient and Nusselt number at $r = 0.5$ and decreases them at $r = 2$. The increase in the ratio of thermal diffusivity, the skin friction coefficient and the rate of heat transfer at both ends increases. The increase in the ratio of viscosity causes an enhancement in the Nusselt number on both the walls and decreases the skin friction coefficient at the wall $r = 2$. The increase in the other parameters like Gt_1, N, P_1, δ_1 has a similar effect on the Nusselt number and the skin friction coefficient. The increase in these parameters increases the Nusselt number and the skin friction coefficient at the wall $r = 0.5$ and decreases them at the wall $r = 2$.

6. Conclusion

The multilayer vertical flow of water and kerosene-based nanofluids has been investigated in the presence of the chemical reaction parameter. The governing equations of this study were non-dimensionalised using suitable relations and the resulting system of equations was solved using the differential transformation method. The outcomes of the study are interpreted through graphs and tables as described in the results and discussion. The key outcomes of the study can be summarised as below:

- The usage of the multilayer model developed in this study helps in maintaining an optimum temperature in the system.

- The region where hybrid nanofluid is considered exhibits higher conduction of heat when compared with the other two regions.
- The thermal and mass Grashof number are found to enhance the flow velocity and the skin friction coefficient.
- The presence of porosity in the middle region helps in controlling the fluid flow.
- It has been found that an increase in the Eckert number enhances the temperature of the nanofluid due to internal heating.
- The increase in the mass diffusivity ratio enhances the mass transfer of the fluid in the middle region and improving the ratio of viscosity enhances the fluid flow.

Disclosure statement

No potential conflict of interest was reported by the author(s).

ORCID

V. Puneeth http://orcid.org/0000-0003-4470-6884

References

Abbas, F., H. M. Ali, M. Shaban, M. M. Janjua, T. R. Shah, M. H. Doranehgard, M. Ahmadlouy-darab, and F. Farukh. 2021. "Towards Convective Heat Transfer Optimization in Aluminum Tube Automotive Radiators: Potential Assessment of Novel $Fe_2O_3 - TiO_2$/water Hybrid Nanofluid." *Journal of the Taiwan Institute of Chemical Engineers* 6 (2): 92–106.

Abbas, Z., and J. Hasnain. 2017. "Two-phase Magneto Convection Flow of Magnetite (Fe_3O_4) Nanoparticles in a Horizontal Composite Porous Annulus." *Results in Physics* 7: 574–580.

Abd-Allah, A. A., and N. Alsedais. 2021. "Magnetic Impact on Heat and Mass Transfer Utilizing Nanofluid in an Annulus Between a Super Ellipse Obstacle and a Cavity with Periodic Side-wall Temperature and Concentration." *Communications in Theoretical Physics* 73: 115001.

Abo-Dahab, S., M. Abdelhafez, F. Mebarek-Oudina, and S. Bilal. 2021. "MHD Casson Nanofluid Flow Over Non-linearly Heated Porous Medium in Presence of Extending Surface Effect with Suction/injection." *Indian Journal of Physics* 95: 1–15.

Al-Farhany, K., and A. D. Abdulsahib. 2021. "Study of Mixed Convection in Two Layers of Saturated Porous Medium and Nanofluid with Rotating Circular Cylinder." *Progress in Nuclear Energy* 135 (19): 103723.

Banisharif, A., P. Estellé, A. Rashidi, S. Van Vaerenbergh, and M. Aghajani. 2021. "Heat Transfer Properties of Metal, Metal Oxides, and Carbon Water Based Nanofluids in the Ethanol Condensation Process." *Colloids and Surfaces A: Physicochemical and Engineering Aspects* 622: 126720.

Chamkha, A. J. 2000. "Flow of Two-immiscible Fluids in Porous and Non Porous Channels." *Journal of Fluids Engineering* 122 (1): 117–124.

Chen, C.-L., and Y. Liu. 2014. "Solution of Two-point Boundary-value Problems Using the Differential Transformation Method." *Journal of Optimization Theory and Applications* 99 (1): 23.

Choi, T. J., M. S. Park, S. H. Kim, and S. P. Jang. 2021. "Experimental Study on the Effect of Nanoparticle Migration on the Convective Heat Transfer Coefficient of EG/water-based Al_2O_3 Nanofluids." *International Journal of Heat and Mass Transfer* 169: 120903.

Ebrahimi, D., S. Yousefzadeh, O. A. Akbari, F. Montazerifar, S. A. Rozati, S. Nakhjavani, and M. R. Safaei. 2021. "Mixed Convection Heat Transfer of a Nanofluid in a Closed Elbow-shaped Cavity (CESC)." *Journal of Thermal Analysis and Calorimetry* 144 (6): 295–2316.

El-Shorbagy, M., F. Eslami, M. Ibrahim, P. Barnoon, W.-F. Xia, and D. Toghraie. 2021. "Numerical Investigation of Mixed Convection of Nanofluid Flow in a Trapezoidal Channel with Different Aspect Ratios in the Presence of Porous Medium." *Case Studies in Thermal Engineering* 25: 100977.

Farooq, M., M. I. Khan, M. Waqas, T. Hayat, A. Alsaedi, and M. I. Khan. 2016. "MHD Stagnation Point Flow of Viscoelastic Nanofluid with Non-linear Radiation Effects." *Journal of Molecular Liquids* 221: 1097–1103.

Fazeli, I., M. R. S. Emami, and A. Rashidi. 2021. "Investigation and Optimization of the Behavior of Heat Transfer and Flow of MWCNT-CuO Hybrid Nanofluid in a Brazed Plate Heat Exchanger Using Response Surface Methodology." *International Communications in Heat and Mass Transfer* 122 (3): 105175.

Hayat, T., A. Shafiq, and A. Alsaedi. 2014. "Effect of Joule Heating and Thermal Radiation in Flow of Third Grade Fluid Over Radiative Surface." *PloS One* 9 (1): e83153.

Hayat, T., A. Shafiq, A. Alsaedi, and S. Asghar. 2015. "Effect of Inclined Magnetic Field in Flow of Third Grade Fluid with Variable Thermal Conductivity." *AIP Advances* 5: 087108.

Kumar, J. P., J. C. Umavathi, A. J. Chamkha, and I. Pop. 2010. "Fully-developed Free-convective Flow of Micropolar and Viscous Fluids in a Vertical Channel." *Applied Mathematical Modelling* 34 (5): 1175–1186.

Malashetty, M., J. Umavathi, and J. P. Kumar. 2004. "Two Fluid Flow and Heat Transfer in An Inclined Channel Containing Porous and Fluid Layer." *Heat and Mass Transfer* 40 (11): 871–876.

Manjunatha, S., B. A. Kuttan, S. Jayanthi, A. J. Chamkha, and B. J. Gireesha. 2019. "Heat Transfer Enhancement in the Boundary Layer Flow of Hybrid Nanofluids Due to Variable Viscosity and Natural Convection." *Heliyon* 5 (4): e01469.

Manjunatha, S., V. Puneeth, R. Anandika, and B. J. Gireesha. 2021. "Analysis of Multilayer Convective Flow of a Hybrid Nanofluid in Porous Medium Sandwiched Between the Layers of Nanofluid." *Heat Transfer* 50: 8598–8616.

Manjunatha, S., V. Puneeth, B. J. Gireesha, and A. J. Chamkha. 2021. "Theoretical Study of Convective Heat Transfer in Ternary Nanofluid Flowing Past a Stretching Sheet." *Journal of Applied and Computational Mechanics* 128: 240–250.

Miles, A., and R. Bessaih. 2021. "Heat Transfer and Entropy Generation Analysis of Three-dimensional Nanofluids Flow in a Cylindrical Annulus Filled with Porous Media." *International Communications in Heat and Mass Transfer* 124: 105240.

Mirzaie, M., and E. Lakzian. 2021. "Natural Convection of Nanofluid-filled Annulus with Cooled and Heated Sources and Rotating Cylinder in the Water Near the Density Inversion Point." *The European Physical Journal Plus* 136 (8): 1–20.

Nallusamy, S. 2016. "Thermal Conductivity Analysis and Characterization of Copper Oxide Nanofluids Through Different Techniques." *Journal of Nano Research* 40: 105–112.

Nallusamy, S., M. Rajaram Narayanan, and J. Logeshwaran. 2017. "Synthesis and Machining Characterization of Copper-multiwalled Carbon Nanotubes-graphene Hybrid Composite Using SEM and ANOVA." *Journal of Nano Research* 50: 105–115.

Naseem, A., A. Shafiq, L. Zhao, and M. U. Farooq. 2018. "Analytical Investigation of Third Grade Nanofluidic Flow Over a Riga Plate Using Cattaneo-Christov Model." *Results in Physics* 9: 961–969.

Odibat, Z. M. 2008. "Differential Transform Method for Solving Volterra Integral Equation with Separable Kernels." *Mathematical and Computer Modelling* 48 (7-8): 7–8.

Rajeev, A., and B. Mahanthesh. 2021. "Multilayer Flow and Heat Transport of Nanoliquids with Nonlinear Boussinesq Approximation and Viscous Heating Using Differential Transform Method." *Heat Transfer* 50 (5): 4309–4327.

Ramesh, G. K., S. Manjunatha, G. S. Roopa, and A. J. Chamkha. 2020. "Hybrid (ND $- CO_3O_4$/EG)nanoliquid Through a Permeable Cylinder Under Homogeneous-heterogeneous Reactions and Slip Effects." *Journal of Thermal Analysis and Calorimetry* 146: 1–11.

Said, Z., M. Ghodbane, L. S. Sundar, A. K. Tiwari, M. Sheikholeslami, and B. Boumeddane. 2021. "Heat Transfer, Entropy Generation, Economic and Environmental Analyses of Linear Fresnel Reflector Using Novel rGo $- CO_3O_4$ Hybrid Nanofluids." *Renewable Energy* 165: 420–437.

Shafiq, A., A. B. Çolak, and T. N. Sindhu. 2021. "Designing Artificial Neural Network of Nanoparticle Diameter and Solid-fluid Interfacial Layer on Single-walled Carbon Nanotubes/ethylene Glycol Nanofluid Flow on Thin Slendering Needles." *International Journal for Numerical Methods in Fluids*93: 3384–3404.

Shafiq, A., Z. Hammouch, and T. N. Sindhu. 2017. "Bioconvective MHD Flow of Tangent Hyperbolic Nanofluid with Newtonian Heating." *International Journal of Mechanical Sciences* 133 (1): 1–11.

Shafiq, A., S. A. Lone, T. N. Sindhu, Q. M. Al-Mdallal, and G. Rasool. 2021. "Statistical Modeling for Bioconvective Tangent Hyperbolic Nanofluid Towards Stretching Surface with Zero Mass Flux Condition." *Scientific Reports* 11 (1): 1–11.

Shafiq, A., F. Mebarek-Oudina, T. N. Sindhu, and A. Abidi. 2021. "A Study of Dual Stratification on Stagnation Point Walters' B Nanofluid Flow Via Radiative Riga Plate: A Statistical Approach." *The European Physical Journal Plus* 136 (4): 1–24.

Shafiq, A.B., T. N. Sindhu, Q. M. Al-Mdallal, and T. Abdeljawad. 2014. "Estimation of Unsteady Hydromagnetic Williamson Fluid Flow in a Radiative Surface Through Numerical and Artificial Neural Network Modeling." *Scientific Reports* 11 (1): 1–21.

Shahsavar, A., S. Noori, D. Toghraie, and P. Barnoon. 2021. "Free Convection of Non-Newtonian Nanofluid Flow Inside An Eccentric Annulus From the Point of View of First-law and Second-law of Thermodynamics." *ZAMM-Journal of Applied Mathematics and Mechanics/Zeitschrift Für Angewandte Math-ematik Und Mechanik* 101 (5): 202000266.

Shahsavar, A., M. Rashidi, C. Yıldız, and M. Arıcı. 2021. "Natural Convection and Entropy Generation of Ag-water Nanofluid in a Finned Horizontal Annulus: A Particular Focus on the Impact of Fin Numbers." *International Communications in Heat and Mass Transfer* 125: 105349.

Umavathi, J., A. J. Chamkha, and M. Shekar. 2014. "Flow and Heat Transfer of Two Micropolar Fluids Separated by a Viscous Fluid Layer." *International Journal of Microscale and Nanoscale Thermal and Fluid Transport Phenomena* 5 (1): 23.

Vajravelu, K., P. Arunachalam, and S. Sreenadh. 1995. "Unsteady Flow of Two Immiscible Conducting Fluids Between Two Permeable Beds." *Journal of Mathematical Analysis and Applications* 196 (2): 1105–1116.

Valizadeh Ardalan, M., R. Alizadeh, A. Fattahi, N. Adelian Rasi, M. H. Doranehgard, and N. G. Karimi. 2021. "Analysis of Unsteady Mixed Convection of Cu–water Nanofluid in An Oscillatory, Lid-driven Enclosure Using Lattice Boltzmann Method." *Journal of Thermal Analysis and Calorimetry* 145 (4): 2045–2061.

Yadav, D., Y.-M. Chu, and Z. Li. 2021. "Examination of the Nanofluid Convective Instability of Vertical Constant Through Flow in a Porous Medium Layer with Variable Gravity." *Applied Nanoscience* 31: 1–14.

Ying, Z., B. He, L. Su, and Y. Kuang. 2021. "Thermo-hydraulic Analyses of the Absorber Tube with Molten Salt-based Nanofluid and Porous Medium Inserts." *Solar Energy* 226: 0–30.

Zari, I., A. Shafiq, G. Rasool, T. N. Sindhu, and T. S. Khan. 2021. "Double-stratified Marangoni Boundary Layer Flow of Casson Nanoliquid: Probable Error Application." *Journal of Thermal Analysis and Calorimetry* 145 (1): 1–17.

Appendix

$$A_1 = \frac{1}{(1-\Phi_{np_1})^{2.5}}$$

$$A_2 = \frac{1}{\left[1-(\Phi_{np_1}+\Phi_{np_2})\right]^{2.5}}$$

$$A_3 = \left[(1-\Phi_{np_1}) + \Phi_{np_1}\frac{(\rho_1)_{np_1}}{(\rho_1)_{bf}}\right]$$

$$A_4 = \left[(1-(\Phi_{np_1}+\Phi_{np_2})) + \Phi_{np_1}\frac{(\rho_2)_{np_1}}{(\rho_2)_{bf}} + \Phi_{np_2}\frac{(\rho_2)_{np_2}}{(\rho_2)_{bf}}\right]$$

$$A_5 = \left[(1-\phi) + \phi_{np_1}\frac{(\rho_1\beta_t)_{np_1}}{(\rho_1\beta_t)_{bf}}\right]$$

$$A_6 = \left[(1-(\Phi_{np_1}+\Phi_{np_2})) + \Phi_{np_1}\frac{(\rho_2\beta_t)_{np_1}}{(\rho_2\beta_t)_{bf}} + \Phi_{np_2}\frac{(\rho_2\beta_t)_{np_2}}{(\rho_2\beta_t)_{bf}}\right]$$

$$A_7 = \left[(1-\Phi_{np_1}) + \Phi_{np_1}\frac{(\rho_1 Cp_1)_{np_1}}{(\rho_1 Cp_1)_{bf}}\right]$$

$$A_8 = \left[(1-(\Phi_{np_1}+\Phi_{np_2})) + \Phi_{np_1}\frac{(\rho_2 Cp_2)_{np_1}}{(\rho_2 Cp_2)_{bf}} + \Phi_{np_2}\frac{(\rho_2 Cp_2)_{np_2}}{(\rho_2 Cp_2)_{bf}}\right]$$

$$A_9 = \frac{(k_{np_1}+2k_{1bf}) - 2\Phi_{np_1}(k_{1bf}-k_{np_1})}{(k_{np_1}+2k_{1bf}) + 2\Phi_{np_1}(k_{1bf}-k_{np_1})}$$

$$A_{10} = \frac{\begin{array}{c}(\frac{\Phi_{np_2}k_{np_2}+\Phi_{np_1}k_{np_1}}{(\Phi_{np_1}+\Phi_{np_2})}) \\ +2k_{2bf}+2\left[\Phi_{np_2}k_{np_2}+\Phi_{np_1}k_{np_1}\right] \\ -2(\Phi_{np_1}+\Phi_{np_2})k_{2bf}\end{array}}{\begin{array}{c}(\frac{\Phi_{np_2}k_{np_2}+\Phi_{np_1}k_{np_1}}{(\Phi_{np_1}+\Phi_{np_2})}) + 2k_{2bf} \\ -\left[\Phi_{np_2}k_{np_2}+\Phi_{np_1}k_{np_1}\right] \\ +(\Phi_{np_1}+\Phi_{np_2})k_{2bf}\end{array}}$$

$$A_{11} = \left[(1-\phi) + \phi_{np_1}\frac{(\rho_1\beta_c)_{np_1}}{(\rho_1\beta_c)_{bf}}\right]$$

$$A_{12} = \left[(1-(\Phi_{np_1}+\Phi_{np_2})) + \Phi_{np_1}\frac{(\rho_2\beta_c)_{np_1}}{(\rho_2\beta_c)_{bf}} + \Phi_{np_2}\frac{(\rho_2\beta_c)_{np_2}}{(\rho_2\beta_c)_{bf}}\right]$$